PROCEEDINGS A

rspa.royalsocietypublishing.org

Research

Cite this article: Kirane K, Su Y, Bažant ZP. 2015 Strain-rate-dependent microplane model for high-rate comminution of concrete under impact based on kinetic energy release theory. *Proc. R. Soc. A* **471**: 20150535.
http://dx.doi.org/10.1098/rspa.2015.0535

Received: 3 August 2015
Accepted: 18 September 2015

Subject Areas:
materials science, civil engineering, structural engineering

Keywords:
projectile impact, dynamic overstress, strain-rate effects, material fragmentation, finite-element simulation, crack band model

Author for correspondence:
Zdeněk P. Bažant
e-mail: z-bazant@northwestern.edu

Strain-rate-dependent microplane model for high-rate comminution of concrete under impact based on kinetic energy release theory

Kedar Kirane[1], Yewang Su[1,2] and Zdeněk P. Bažant[1]

[1]Department of Civil and Environmental Engineering, Northwestern University, 2145 Sheridan Road, Evanston, IL 60208, USA
[2]State Key Laboratory of Nonlinear Mechanics, Institute of Mechanics, Chinese Academy of Sciences, Beijing 100190, People's Republic of China

The apparent increase of strength of concrete at very high strain rates experienced in projectile impact ($10\,s^{-1}$ to $10^6\,s^{-1}$), called 'dynamic overstress', has recently been explained by the theory of release of local kinetic energy of shear strain rate in finite size particles about to form. This theory gives the particle size and the additional kinetic energy density that must be dissipated in finite-element codes. In previous research, it was dissipated by additional viscosity, in a model partly analogous to turbulence theory. Here it is dissipated by scaling up the material strength. Microplane model M7 is used and its stress–strain boundaries are scaled up by factors proportional to the −4/3rd power of the effective deviatoric strain rate and its time derivative. The crack band model with a random tetrahedral mesh is used and all the artificial damping is eliminated. The scaled M7 model is seen to predict the crater shapes and exit velocities of projectiles penetrating concrete walls of different thicknesses as closely as the previous models. The choice of the finite strain threshold for element deletion criterion, which can have a big effect, is also studied. It is proposed to use the highest threshold above which a further increase has a negligible effect.

THE ROYAL SOCIETY PUBLISHING

1. Introduction

Dynamic fracture has been the subject of numerous studies [1–21]. Many aspects are now well understood, especially the dynamic propagation and branching of individual cracks [2,5,17,19, 22,23]. The dynamic comminution (i.e. fragmentation, pulverization and crushing) is of interest for many practical purposes, including impact of rocks, concrete, metals, composites and ceramics [3–5,17,21], as well as various industrial grain reduction processes, explosion effects on structures, rock blasting and fracturing of gas or oil shale by chemical explosions or by electro-hydraulic pulsed arc in a horizontal borehole [24,25]. This paper is focused on only one aspect—the projectile impact onto concrete walls.

Predictability of impact effects on concrete has been hampered by the problem of the so-called 'dynamic overstress'. As the strain rate increases above $1\,s^{-1}$, the material strength needed to fit data on projectile penetration appears to increase above what is predicted by the standard rate effects, which include the activation energy controlled bond breakage at crack tips and viscoelasticity of the material between the cracks. At strain rates above $10^4\,s^{-1}$, this increase becomes enormous (e.g. [26]). Some investigators [7] dealt with this problem by simply adjusting the strain-dependent strength limits (or boundaries) of microplane model M4 so as to fit the exit velocities of a projectile penetrating a wall. Lacking physical justification, such an approach cannot be expected to be predictive in different situations.

In [27,28], it was proposed that the physical justification of 'dynamic overstress' must be sought in the fracturing of concrete which is driven not by the release of strain energy, as in classical fracture mechanics, but by the release of kinetic energy of shear strain rate field within forming particles as the concrete is getting comminuted into small fragments. At the rate of $10^4\,s^{-1}$, the kinetic energy of the forming particle exceeds the maximum possible strain energy in the particle by two orders of magnitude. Thus the comminution process can dissipate a lot of energy [11–15], is not covered by the damage constitutive laws based on standard triaxial testing which leads to much larger fragments. This new theory, which bears some analogy to turbulence, was shown to give a strain-rate-dependent expression for the additional density $\Delta\mathcal{K}$ of kinetic energy that drives the comminution and must be dissipated in the finite-element code. There are various methods to dissipate it, and apparently it does not matter which one is adopted.

(1) One method to dissipate $\Delta\mathcal{K}$, which is more natural for rate-dependent stress, is to introduce additional shear viscosity η calculated from the calculated kinetic energy release. This led to a model with partial analogy to turbulence theory [27,29]. As a simplified approach, η was considered to depend only on the strain rate [27,28]. In a rigorous approach, η was considered to also depend on the strain-rate derivative [30]. Both approaches led to a good match of test data on the exit velocities of projectiles from concrete walls of different thicknesses, and the latter also matched well the measured penetration depths of projectiles of different velocities.

(2) As another method, rather than treating the interface fracture between forming particles as instantaneous, it was considered to grow at a finite (though very high) speed, according to a power law of kinetic energy release rate, similar to the Charles–Evans law for static subcritical crack growth. In this way, the same data could again be matched well [31].

(3) A third method, which can match the data on projectile exit velocity and penetration depths equally well, is studied here. Similar to [7], the strain-dependent strength limits (called boundaries) of the microplane damage constitutive model M7 are raised as a function of the shear strain rate, but not by a factor found [7] by matching the projectile penetration data, which would not be predictive. Rather, they are raised so as to dissipate the additional kinetic density $\Delta\mathcal{K}$ of the shear strain rate field in the forming particles. It is also assumed that the particles form instantly, as in method 1. This method leads to strength increase depending on both the strain rate and its derivative. The post-comminution behaviour, including subsequent further comminution and clustering into

bigger particle groups to release the kinetic energy that is being dissipated by inter-group friction, is also discussed and modelled. The present formulation makes it possible to eliminate the artificial dampings of all types, which are normally embedded in commercial finite-element codes but are not predictive as they are not justified physically.

In an attempt to handle the 'dynamic overstress', an increase of the microplane stress–strain boundaries (or strength limits) was already introduced by Adley *et al.* [7,8] (using model M4). They scaled the boundaries as a function of the strain rate $\dot{\epsilon}$ by a rate amplification factor χ given as,

$$\chi_i = \dot{\epsilon}_{\text{norm}}^{c_i}, \quad \text{where} \quad \dot{\epsilon}_{\text{norm}} = \max\left(\frac{\dot{\epsilon}}{\dot{\epsilon}_{\text{quasistatic}}}, 1.0\right), \tag{1.1}$$

where c_i are empirical exponents, different for each boundary. They obtained these exponents by fitting the missile penetration data. They achieved a good fit of the observed exit velocities of projectiles penetrating concrete walls of different thicknesses, as well as the crater shapes. However, the connection to the data from quasi-static material testing of concrete, which is the only available source of nonlinear triaxial, damage and fracture properties, was thus lost. The modified microplane model used in these impact simulations could not fit the material test data. Therefore, the model cannot be predictive for other situations.

2. Brief overview of the kinetic energy theory of comminution

The physical source of 'dynamic overstress' during impact was traced to the dissipation of the local kinetic energy of shear strain rate within finite size comminuting particles [27]. Let ϵ_{Dij} denote the deviatoric strain tensor and the superior dot the derivatives with respect to time t. Then, the density of kinetic energy of effective deviatoric strain rate $\dot{\epsilon}_D = \sqrt{\dot{\epsilon}_{Dij}\dot{\epsilon}_{Dij}/2}$ is dissipated by creating interface fractures resulting in many particles.

Consider an idealized dynamic fracture process in which the solid is comminuted to identical prismatic particles of length h and hexagonal cross-section of side $h/2$, at a deviatoric strain rate $\dot{\epsilon}_D$ (figure 1). Analysis of the kinematics and comparison of the kinetic energy of particles before (figure 1*b*) and after (figure 1*c*) the interface fracture showed [27] that, for a motion in the plane of maximum shear strain, the local kinetic energy of the particles that are about to form, per unit volume of material, $\Delta\mathcal{K}$, is additive to, and separable from, the global kinetic energy.

The global kinetic energy corresponds to the motion of the centres of the particles whose formation is imminent. For a given $\dot{\epsilon}_D$, the drop in kinetic energy per unit volume is found to be [27]:

$$-\Delta\mathcal{K} = c_k \rho h^2 \dot{\epsilon}_D^2, \tag{2.1}$$

where $c_k = I_p/(2hV_p)$, $\rho =$ mass density, $V_p = 3\sqrt{3}h^3/8$ and $I_p = 5\sqrt{3}h^4/128 =$ volume and polar moment of inertia of each hexagonal prism about its axis, respectively.

In reality, the size of comminuted particles is never uniform but varies randomly within a certain range, $s \in (h, H)$ where $h, H =$ minimum and maximum sizes, and $s =$ variable particle size. Schuhmann's empirical power law [32] is adopted to describe the cumulative distribution. It gives the volume fraction of particles of sizes between h to s:

$$F(s) = \frac{s^k - h^k}{H^k - h^k}, \quad s \in (h, H), F(s) \in (0, 1), \tag{2.2}$$

where ($k \approx 0.5$) is the empirical constant [27].

Then, introducing the simplifying hypothesis that the kinetic energy drop for variable particle size can be obtained by summing the energy losses for all infinitesimal intervals $(s, s + \mathrm{d}s)$ calculated for each interval as if the particle size and shape were uniform. Integration furnishes

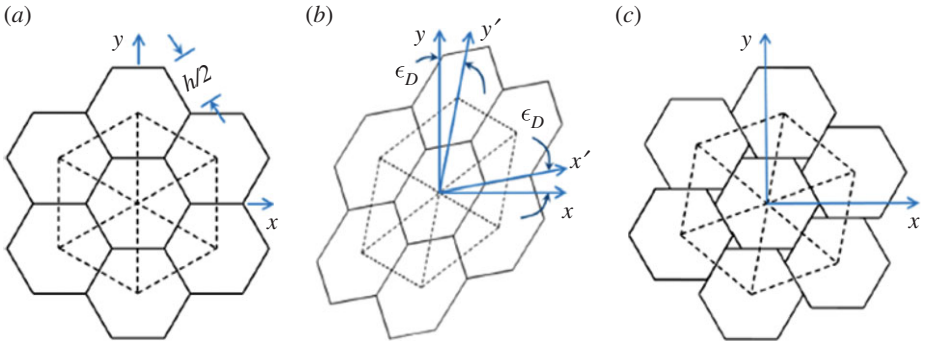

Figure 1. Schematic of material comminution into prismatic hexagonal particles: (*a*) undeformed regime; (*b*) sheared regime and (*c*) comminuted regime. (Online version in colour.)

the kinetic energy drop for particles of all sizes per unit volume [27]:

$$-\Delta\mathcal{K} = \int_{s=h}^{H} c_k \rho s^2 \dot{\epsilon}_D^2 \, \mathrm{d}F(s) = C_k \rho h^2 \dot{\epsilon}_D^2, \tag{2.3}$$

where

$$C_k = \frac{k}{k+2} \frac{(H/h)^{k+2} - 1}{(H/h)^k - 1} \, c_k. \tag{2.4}$$

The interface area of uniform particles of size s per unit volume of material is c_s/s, where c_s is the dimensionless constant. For particle size distributed according to equation (2.2), the particle interface area per unit volume of material is obtained as [27]:

$$S = \int_{s=h}^{H} \frac{c_s}{s} \, \mathrm{d}F(s) = \frac{C_s}{h}, \tag{2.5}$$

where

$$C_s = \frac{c_s k}{k-1} \frac{(H/h)^{k-1} - 1}{(H/h)^k - 1} \tag{2.6}$$

is a dimensionless constant [27]. Equation (2.5) adds, or integrates, the energy dissipations for different particle sizes and is calculated under the assumption that for each size there is a regular array of equal-size particles.

Then, considering the dynamic fracture criterion [27,30] to be $-\Delta\mathcal{K} = S\Gamma$, an overall energy balance is imposed (where Γ is the interface fracture energy of the comminuting particles). Substitution of equations 2.3 and 2.5 gives the minimum particle size as

$$h = C_r \left(\frac{\Gamma}{\rho \dot{\epsilon}_D^2} \right)^{1/3}, \tag{2.7}$$

where

$$C_r = \left(\frac{c_s}{c_k} \frac{k+2}{k-1} \frac{(H/h)^{k-1} - 1}{(H/h)^{k+2} - 1} \right)^{1/3}, \tag{2.8}$$

where C_r is a dimensionless constant. As seen in equation (2.7), the particle size is proportional to the $\frac{-2}{3}$ power of the effective deviatoric strain rate. A higher effective deviatoric strain rate gives a greater kinetic energy release, which leads to smaller particles, and thus to a greater interface area and more dissipation.

In [27], equation 2.8 was used as an explicit formula in which the value of H/h was estimated. It should be noted that this estimate might have some errors. An alternate approach could be using a variable H/h, where H is constant but h is not. But this would require a reformulation

of the theory and could not be used in arriving at equation (2.7). Such a theory might be more complicated without a significant improvement in predictions. Hence, we assume a constant H/h.

Then, substitution of equation (2.7) into equation (2.3) gives the kinetic energy drop in terms of only the effective deviatoric strain rate and the material parameters:

$$-\Delta\mathcal{K} = A\dot{\epsilon}_D^{2/3}, \tag{2.9}$$

where $A = (C_0\Gamma^2\rho)^{1/3}$ and $C_0 = C_k^3 C_r^2$ is a dimensionless constant. Note that assuming a hexagonal shape of particles is not a strict requirement of the formulation. In reality the shapes of the particles are sure to be variable, but the basic functional form of the equations is not expected to change.

Furthermore, note that in an actual impact event, $\dot{\epsilon}_D$ need not be constant during comminution of a given material volume. So it is useful to obtain the drop in kinetic energy in one time increment of the comminution process. Accordingly, as proposed in [30] the increment of drop in kinetic energy is given by

$$\mathrm{d}(-\Delta\mathcal{K}) = \frac{2A}{3}\,\dot{\epsilon}_D^{-1/3}\mathrm{d}\dot{\epsilon}_D. \tag{2.10}$$

Thus, in a given strain increment, the drop in kinetic energy depends not only on the strain rate but also its increment. Any scaling of the boundaries of a constitutive model to account for comminution, must be consistent with this dependence. Such a formulation is proposed in the next section, for the microplane model M7.

3. Microplane model M7 with scaled boundaries

The microplane model M7 is the latest version in a series of progressively improved microplane models labelled M0, M1, M2, …, M6, developed first for concrete (and then extended to other materials). The microplane model, supplemented by some localization limiter with material characteristic length, has been proven to give rather realistic predictions of the constitutive and damage behaviour of quasi-brittle materials over a broad range of loading scenarios, including uniaxial, biaxial and triaxial loadings with post-peak softening, compression-tension load cycles, opening and mixed mode fractures, tension-shear failure and axial compression followed by torsion [33,34].

The basic idea of the microplane model is to express the constitutive law not in terms of tensors, but in terms of the vectors of stress and strain acting on a generic plane of any orientation in the material microstructure, called the microplane. The use of vectors is analogous to the Taylor models used for plasticity of polycrystalline metals, but with important conceptual differences. Firstly, to avoid model instability in post-peak softening, a kinematic constraint is used instead of a static one [33]. Thus, the strain (rather than stress) vector on each microplane is the projection of the macroscopic strain tensor. So we have,

$$\epsilon_\mathrm{N} = \epsilon_{ij}N_{ij}, \quad \epsilon_\mathrm{M} = \epsilon_{ij}M_{ij} \quad \text{and} \quad \epsilon_\mathrm{L} = \epsilon_{ij}L_{ij}, \tag{3.1}$$

where ϵ_N, ϵ_M and ϵ_L are the magnitudes of the three strain vectors corresponding to each microplane, and $N_{ij} = n_i n_j$, $M_{ij} = (n_i m_j + m_i n_j)/2$ and $L_{ij} = (n_i l_j + l_i n_j)/2$, n, m, and l being the three mutually orthogonal normal and tangential unit vectors characterizing that microplane, and the subscripts i and $j = 1,2,3$. Secondly, a variational principle (principle of virtual work) relates the stresses on the microplanes (σ_N, σ_M and σ_L) to the macro-continuum stress tensor σ_{ij}, to ensure equilibrium; it is expressed as

$$\frac{2\pi}{3}\sigma_{ij}\delta\epsilon_{ij} = \int_\Omega (\sigma_\mathrm{N}\delta\epsilon_\mathrm{N} + \sigma_\mathrm{M}\delta\epsilon_\mathrm{M} + \sigma_\mathrm{L}\delta\epsilon_\mathrm{L})\mathrm{d}\Omega. \tag{3.2}$$

This expression means that, within a unit sphere, the virtual works of macro-stresses and micro-stresses must be equal (for details, see [33,35]). In the microplane model M7, the micro-stresses are subjected to strain-dependent boundaries (or strength limits) of four types, *viz.*:

(1) the tensile normal boundary—to capture progressive tensile fracturing;
(2) the compressive volumetric boundary—to capture phenomenon such as pore collapse under extreme pressures;
(3) the compressive deviatoric boundary—to capture softening in compression; and
(4) the shear boundary—to capture friction.

The M7 also includes the quasi-static rate effects [36], which consist of a rate-dependent crack opening and growth controlled by the activation energy of bond breakage, and of visco-elasticity of the material between the cracks. However, the quasi-static rate effects in M7 have been calibrated for strain rates of about $1\,s^{-1}$, and would have to be recalibrated.

As comminution is induced by local shear strains, we assume that in a given strain increment $d\epsilon_{ij}$, the additional energy to be dissipated must equal the additional distortional strain energy given by $\Delta\sigma_{Dij}\epsilon_{Dij}$, where $\Delta\sigma_{Dij}$ is the additional deviatoric stress that results due to scaled boundaries. To express it in terms of the microplane stresses, we first define the volumetric stress on the microplane level, σ_V, as

$$\frac{2\pi}{3}\frac{\sigma_{kk}}{3}\delta\epsilon_{mm} = \int_\Omega \sigma_V \delta\epsilon_V d\Omega. \tag{3.3}$$

Substituting $\delta\epsilon_V = \delta\epsilon_{mm}/3$ and $\int_\Omega = 2\pi d\Omega$, the volumetric stress on the microplane level can be expressed as $\sigma_V = \sigma_{kk}/3$. Also, the microplane normal stresses $\sigma_N = \sigma_D + \sigma_V$, where σ_D is the deviatoric stress on the microplane level. Likewise, for microplane strains, we have $\epsilon_N = \epsilon_D + \epsilon_V$. Note that $\epsilon_V = \epsilon_{kk}/3$ is the same for all microplanes. Then, subtracting equation (3.3) from (3.2), we get

$$\frac{2\pi}{3}\left(\sigma_{ij} - \frac{\sigma_{kk}}{3}\right)\delta\epsilon_{ij} = \int_\Omega (\sigma_D + \sigma_V)(\delta\epsilon_D + \delta\epsilon_V) + \sigma_M\delta\epsilon_M + \sigma_L\delta\epsilon_L - \sigma_V\delta\epsilon_V d\Omega. \tag{3.4}$$

Now noting that $\int_\Omega \sigma_D\delta\epsilon_V = \int_\Omega \sigma_V\delta\epsilon_D = 0$, we get

$$\frac{2\pi}{3}\sigma_{Dij}\delta\epsilon_{ij} = \int_\Omega (\sigma_D\delta\epsilon_D + \sigma_M\delta\epsilon_M + \sigma_L\delta\epsilon_L) d\Omega. \tag{3.5}$$

Then, noting that $\delta\epsilon_D = \delta\epsilon_N - \delta\epsilon_V = \delta\epsilon_{ij}N_{ij} - \delta\epsilon_{ij}\delta_{ij}/3$, $\delta\epsilon_M = \delta\epsilon_{ij}M_{ij}$ and $\delta\epsilon_L = \delta\epsilon_{ij}L_{ij}$, we get an expression for the macroscale deviatoric stress tensor as,

$$\frac{2\pi}{3}\sigma_{Dij} = \int_\Omega \sigma_D\left(N_{ij} - \frac{\delta_{ij}}{3}\right) + \sigma_M M_{ij} + \sigma_L L_{ij} d\Omega. \tag{3.6}$$

This expression implies that a change in the macro-scale deviatoric stress can be achieved by scaling only the deviatoric and frictional boundaries of M7. Let the change in the microplane deviatoric and shear stresses be $\Delta\sigma_D$, $\Delta\sigma_M$ and $\Delta\sigma_L$ for a change in deviatoric stress of $\Delta\sigma_{Dij}$. So we have,

$$\frac{2\pi}{3}\Delta\sigma_{Dij} = \int_\Omega \Delta\sigma_D\left(N_{ij} - \frac{\delta_{ij}}{3}\right) + \Delta\sigma_M M_{ij} + \Delta\sigma_L L_{ij} d\Omega. \tag{3.7}$$

Now, in the interest of simplicity, we assume that both the deviatoric and frictional boundaries are scaled by the same amount, on each microplane. So, $\Delta\sigma_D = \Delta\sigma_M = \Delta\sigma_L = \Delta f$, and

$$\frac{2\pi}{3}\Delta\sigma_{Dij} = \int_\Omega \Delta f\left(N_{ij} - \frac{\delta_{ij}}{3}\right) + \Delta f M_{ij} + \Delta f L_{ij} d\Omega. \tag{3.8}$$

This may be simplified as

$$\Delta\sigma_{Dij} = \Delta f C_{ij}, \tag{3.9}$$

where,

$$C_{ij} = \frac{3}{2\pi}\int_\Omega \left(N_{ij} - \frac{\delta_{ij}}{3}\right) + M_{ij} + L_{ij} d\Omega, \quad \text{which is constant.} \tag{3.10}$$

Δf may be taken out of the integral as we assume it to be the same for each microplane. Now, the next task is to relate the quantity Δf to the energy dissipated due to comminution, $\Delta\mathcal{K}$. To ensure

the aforementioned energy balance, the work of the additional deviatoric stress must dissipate an energy equal to the drop of kinetic energy of strain rate field caused by comminution in each increment. So,

$$d(-\Delta\mathcal{K}) = \Delta\sigma_{Dij}\mathrm{d}\epsilon_{Dij}, \tag{3.11}$$

where $i, j = 1, 2, 3$ and d denotes a small increment. So we have

$$d(-\Delta\mathcal{K}) = \Delta f C_{ij}\mathrm{d}\epsilon_{Dij.} \tag{3.12}$$

Now, using equation 2.10 and taking the derivative with respect to time on both sides, we get

$$\frac{2A}{3}\dot{\epsilon}_{\mathrm{D}}^{-1/3}\ddot{\epsilon}_{\mathrm{D}} = \Delta f\ C_{ij}\dot{\epsilon}_{Dij.} \tag{3.13}$$

Multiplying both sides by $\dot{\epsilon}_{Dij}$, we get

$$\frac{2A}{3}\dot{\epsilon}_{\mathrm{D}}^{-1/3}\ddot{\epsilon}_{\mathrm{D}}\dot{\epsilon}_{Dij} = 2\Delta f\ C_{ij}\dot{\epsilon}_{D}^{2}, \tag{3.14}$$

as $\dot{\epsilon}_{\mathrm{D}} = \sqrt{\dot{\epsilon}_{ij}\dot{\epsilon}_{ij}/2}$. Thus we have,

$$\Delta f\ C_{ij} = \frac{A}{3}\dot{\epsilon}_{\mathrm{D}}^{-7/3}\ddot{\epsilon}_{\mathrm{D}}\dot{\epsilon}_{Dij}. \tag{3.15}$$

Note that the right-hand side of this expression is consistent with [30]. To obtain the scalar value Δf, we now calculate the effective values of both sides, by taking square root of the inner product with itself. So we have

$$\Delta f\ (C_{ij}C_{ij})^{1/2} = \frac{\sqrt{2}A}{3}\dot{\epsilon}_{\mathrm{D}}^{-7/3}\ddot{\epsilon}_{\mathrm{D}}\dot{\epsilon}_{\mathrm{D}}. \tag{3.16}$$

Thus, the scalar Δf is expressed as

$$\Delta f = A_1\dot{\epsilon}_{\mathrm{D}}^{-4/3}\ddot{\epsilon}_{\mathrm{D}}. \tag{3.17}$$

Here A_1 is a constant to be calibrated, and is given by $A_1 = \sqrt{2}A/3\bar{C}$ and $\bar{C} = \sqrt{C_{ij}C_{ij}}$. Therefore, the deviatoric and frictional boundaries of M7 are scaled as $F = F_{\mathrm{qs}}(1 + A_1\dot{\epsilon}_{\mathrm{D}}^{-4/3}\ddot{\epsilon}_{\mathrm{D}})$, where $F_{\mathrm{qs}} = F_0(1 + h(\dot{\epsilon}))$, the boundary that is already scaled to account for the quasi-static rate effects [36], and F_0 is the original unscaled M7 boundary. This expression shows that to capture the energy dissipation due to comminution, it is necessary to make the boundary a function of both the first and second time derivatives of the effective deviatoric strain.

4. Concrete slab perforation by projectile impact

The M7 model with scaled boundaries was evaluated using the tests of projectile perforation, performed at the Geotechnical and Structure Laboratory of the US. Army Engineer Research and Development centre (ERDC), Vicksburg [8,37]. These tests used circular slabs of four thicknesses, 127, 216, 254 and 280 mm, made of concrete WES-5000, whose standard compression strength was 48 MPa. The slabs were cast in steel culvert pipes of diameter 1.52 m, sufficient to approximate the response for a semi-infinite radius (despite that non-reflecting finite elements producing no backward waves were used at the boundary). The projectiles, which were hollow and made of steel, had an ogival-nose (caliber radius head 3.0, length/diameter ratio 7.0 and diameter 50.8 mm) and weight of 2.3 kg. The projectiles impacted the concrete slabs with the velocity of 310 m s^{-1} at the angle of 90°. The perforation tests were carried out two or three times for each thickness of the slab. First, the M7 model was calibrated to fit the test data for concrete WES-5000, used in these tests. This concrete had Young's modulus $E = 25$ GPa, and Poisson's ratio $\mu = 0.18$. The optimum values of M7 parameters, which achieved very good fits of quasi-static uni-, bi- and tri-axial tests, were $k_1 = 11 \times 10^{-5}$, $k_2 = 110$, $k_3 = 30$, $k_4 = 100$ and $k_5 = 10^{-4}$ [33,34].

The mesh used to discretize the slabs was random but statistically uniform, and consisted of tetrahedral elements of average size 7.5 mm. The projectile was considered rigid as no obvious

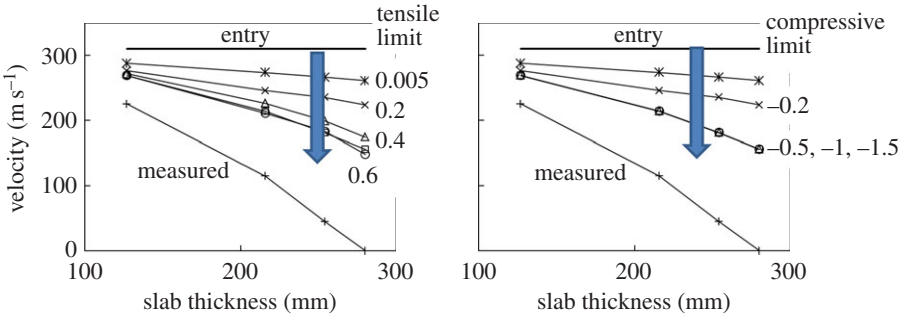

Figure 2. Predicted exit velocities using basic M7 model with no rate effects, for various element deletion thresholds. (Online version in colour.)

damage, melt or deformation was observed after the test. To prevent spurious mesh sensitivity, the modelling was performed in the sense of the crack band model, in which the finite-element size (or mesh size) should be equal to the material characteristic length, which characterizes the size of the representative volume element (RVE) of the material and is used as the localization limiter. The element size was considered as 7.5 mm, which is about one to two times the maximum aggregate size. Note that if, in quasi-static problems, the element size is changed, the crack band model requires adjusting the post-peak softening of the damage constitutive law so that the energy dissipated in the crack band (localized into one element width) would not change [38] (which is what is done in commercial software such as ATENA or OOFEM [39]). But, in projectile impact problems, the deformation is generally so fast that there is not enough time for the cracking damage to localize, and so the post-peak of the damage law need not, and should not, be adjusted.

Also note that, while the apparent strength and fracture energy depend on the strain rate, the crack band width itself does not. It is a material property that can be measured, e.g. as the minimum possible spacing of parallel quasi-static macro-cracks. It depends on material heterogeneity, and is usually equal to 1 to 3 maximum inhomogeneity sizes. In dynamic fracture, where the localization is suppressed by high deformation rates, the finite-element solver based on the crack band model automatically simulates (in a diffuse way, of course) the formation of multiple cracks and crack branching. The additional energy dissipation at very high strain rates is accounted for by material law adjustment, one type of which is presented here.

(a) Element deletion criterion

For these analyses, it was necessary to remove excessively distorted elements to avoid termination of analysis due to a negative Jacobian. This was done using an element deletion criterion based on the maximum principal strain. Thresholds of the criterion were set independently for tension and compression, to a value such that a further increase of the threshold did not make a difference to the predicted exit velocities. Initially, considering the unscaled M7 model, a sensitivity study was conducted using various tensile and compressive threshold values. The results are shown in figure 2*a*,*b*. It can be seen that, beyond 40% tensile strain and 100% compressive strain, the exit velocities do not change much. Accordingly, these values were set as the thresholds for the element deletion criterion. For the sake of comparison, the results using the basic M7 with the element deletion criterion from [28] (tensile threshold = 0.5% and no compressive threshold) and [30] (tensile threshold = 100% and compressive threshold = −20%) are also shown. It is seen that those deletion thresholds led to an overestimation of the exit velocity. This is rectified here by using sufficiently higher thresholds.

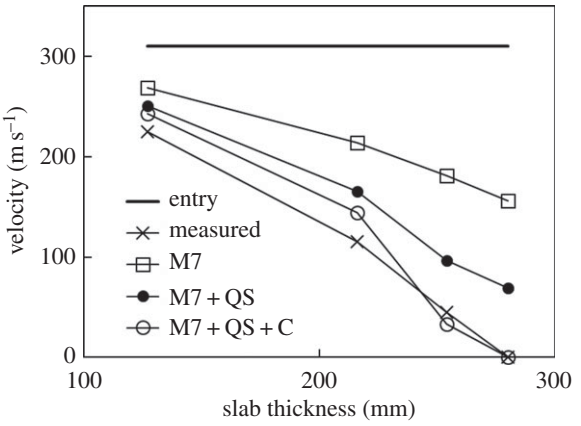

Figure 3. Comparison of the exit velocities predicted by M7 with no rate effects, with quasi-static rate effects and with comminution effects and the experimental data.

(b) Quasi-static rate effects

Next, using the aforementioned element deletion criterion, the quasi-static rate effects were employed, and the projectile exit velocities were predicted (with the same parameters as mentioned in [28]). These effects mainly refer to the rate dependence of cohesive crack opening and follow from the activation energy theory of bond ruptures. These effects are accounted for by scaling all the boundaries of M7 as $F_{qs} = F_0(1 + C_{R2}\ln(2\dot{\epsilon}/C_{R1}))$ [36], where $\dot{\epsilon} = \sqrt{\frac{1}{2}\dot{\epsilon}_{ij}\dot{\epsilon}_{ij}}$. The parameter values C_{R1} and C_{R2} were determined in [28] to be 4×10^{-6} and 0.022, respectively. The exit velocities were again predicted by including these effects, as shown in figure 3. It is seen that these effects caused the predicted velocities to change significantly. In previous studies [28], use of a non-conservative element deletion criterion possibly underestimated the magnitude of these effects, which is again rectified here. However, it is seen that the quasi-static rate effects still do not suffice to correctly predict the exit velocities. So now we add the effects of comminution by scaling the deviatoric and friction boundaries of M7, as described in §3.

(c) Comminution effects

Parameter A_1 was calibrated by fitting one data point in figure 3, which led to the value $A_1 = 3 \times 10^{-7}$. The remaining points were then predicted. Figure 3 shows the predicted exit velocities for all the four slabs tested. As can be seen, the predictions of exit velocities are reasonably good, for all the data points. For the smaller slabs, the exit velocity is slightly overestimated while for the larger slab it is slightly underestimated. The fit could further be improved by relaxing the assumption that both the deviatoric and friction boundaries are scaled by the same factor. But this has not been explored as the errors are small and the data are too limited for calibrating two factors. To further assess the predictions, the predicted crater shapes for the slabs are compared with the measured ones, as shown in figure 4. It can be seen that the shapes can be matched very well, especially those at the exit side. This serves to show that the proposed scaling of M7 boundaries accounts for the phenomenon of comminution quite well.

(d) Finite strain effects

The basic form of microplane model M7 applies only to small strains. In comminution, however, very large strains might occur. To deal with them, a finite strain generalization of the microplane model M4, a predecessor of M7, was proposed in [40]. The same generalization is possible for model M7.

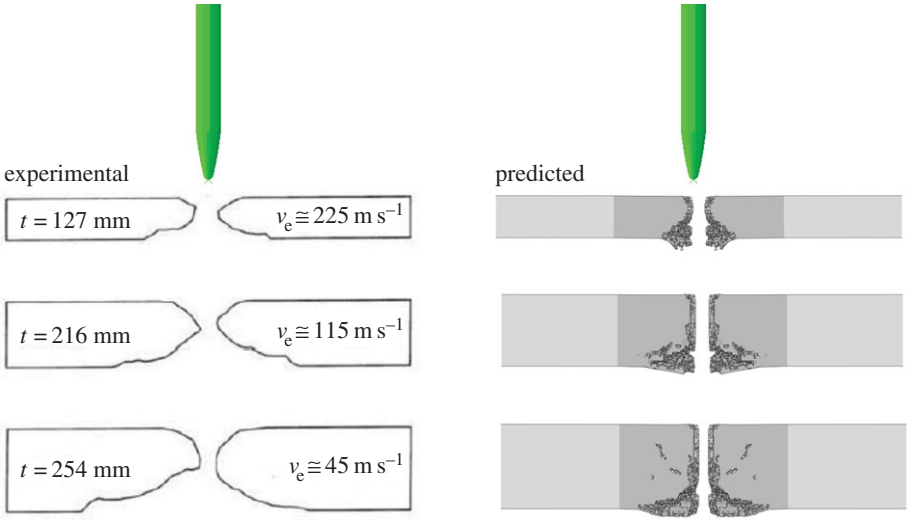

Figure 4. Comparison of the crater shapes predicted by M7 with comminution effects and the experiment data. (Online version in colour.)

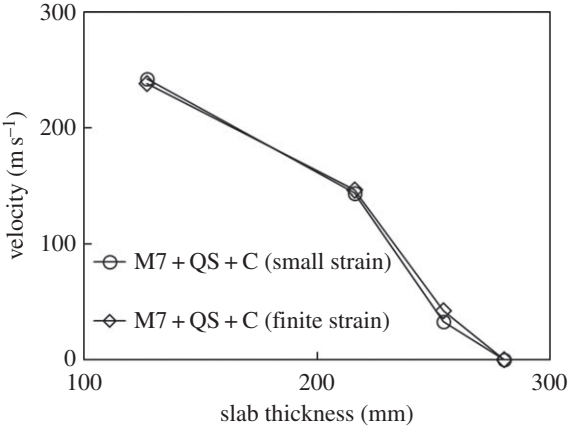

Figure 5. Comparison of the exit velocities predicted by the small and finite strain versions of M7, both include comminution effects.

According to [40], the finite strain generalization of the microplane model is formulated in terms of the stretches and shear angles calculated from the Green–Lagrange strain measure. Only for this strain measure, the stretch in normal direction to one microplane and the shear angles on that microplane can be calculated from the strain components on that same microplane exactly. For other strain measures, they cannot as the stretch and shear angles on one microplane depend also on the strain components on other microplanes. For the Green–Lagrange strain measure, the volumetric strain ϵ_V is obtained as, $\epsilon_V = \epsilon_0 + \epsilon_0^2/2$, where $\epsilon_0 = (J-1)/3$ and $J = \det(F)$, F being the deformation gradient. For large strains, the volumetric–deviatoric split of the strain tensor is in general multiplicative. However, for concrete, the ϵ_V magnitude can hardly exceed 3%, which is small enough to allow additive split, as used in M7 (and earlier in M4 [40]).

The best choice of the stress tensor for this case was shown to be the back-rotated Cauchy stress tensor $S = R^T \sigma R$, where R is the rotation tensor and σ is the Cauchy stress tensor. The Cauchy stress tensors enables the microplane stress vectors to have clear physical meaning, which simplifies the control of hydrostatic pressure sensitivity, internal friction and dilatancy of material. The projectile impact analyses were rerun with this generalization, and included both quasi-static

rate effects, and the kinetic energy rate effect. The finite strain generalization did change the results but not significantly, as seen in figure 5. The reason could be that even though the total strains are high, the rotations are not.

5. Conclusion

(1) The microplane model M7 with boundaries modified according to the kinetic energy theory of comminution is an effective approach to simulate projectile impact effects on concrete slabs and offers possibilities of further refinement. It can accurately predict projectile exit velocities, crater shapes and penetration depths.
(2) It is necessary to scale up the deviatoric and friction boundaries of M7, to achieve a rate-dependent increase of the macroscopic deviatoric stress. Greater versatility could be obtained by scaling up the deviatoric and friction boundaries by different factors. But there are not enough test data to calibrate two independent factors.
(3) The scaling of the boundaries (or strength limits) must be proportional to both: (i) the $-4/3$ power of the effective deviatoric strain rate and (ii) the time derivative of that rate.
(4) The crack band model with a random tetrahedral mesh leads to accurate predictions of the crater shapes.
(5) An element deletion threshold is necessary to run impact analyses. The choice of the threshold has a significant effect on the results. Chosen is a high enough threshold for maximum principal strain such that a further increase would not change the results appreciably.
(6) The finite strain generalization of the microplane model did not have a significant effect on the predicted exit velocities, perhaps because the material rotations were not too high.
(7) What is most important is that the finite-element code dissipate the correct energy required by the kinetic theory of comminution. But how exactly this energy is dissipated does not seem important. Dissipation modes in terms of additional viscosity, rate dependence of interface fracture, and scaling of strength limits give similar results. While the viscosity approach is more natural for rate-dependent stress, the present approach has the advantage of greater versatility for further refinements, such as the possibility of different scalings of different microplane boundaries, which might be needed for various extensions such as hypervelocity impact, impact on rock, or explosive comminution of rock, e.g. shale.

Data accessibility. All the test data used were taken from the open literature.

Authors' contributions. The first author, K.K. developed the formulation of boundary scaling in detail, implemented it as an Abaqus subroutine, conducted the finite-element analyses test data fitting and wrote the first draft of the paper. The second author Y.S. contributed in the development of the formulation via technical discussions, provided the finite-element meshes and also reviewed and improved the draft. The corresponding author Z.P.B. conceived the basic idea of kinetic energy release from finite-size particles, directed the work and finalized the text. All the authors approved the publication.

Conflict of interests. We declare we have no conflicting interests.

Funding. Support under grant no. W911NF-15-1-0240 from the US Army Research Office, Durham, to Northwestern University, is gratefully acknowledged.

Acknowledgements. Thanks are due to Ferhun Caner, Visiting Scholar at Northwestern University, on leave from UPC, Barcelona, for making available his coding of M7 and the meshes for slab perforations. The second author acknowledges the support from Chinese Academy of Sciences via the 'Hundred Talent program' and support from NSFC (No. 11572323)

References

1. Cadoni E, Labibes K, Albertini C, Berra M, Giangrasso M. 2001 Strain-rate effect on the tensile behaviour of concrete at different relative humidity levels. *Mater. Struct.* **34**, 21–26. (doi:10.1007/BF02482196)

2. Camacho G, Ortiz M. 1996 Computational modelling of impact damage in brittle materials. *Int. J. Solids Struct.* **33**, 2899–2938. (doi:10.1016/0020-7683(95)00255-3)
3. Deshpande V, Evans A. 2008 Inelastic deformation and energy dissipation in ceramics: a mechanism-based constitutive model. *J. Mech. Phys. Solids* **56**, 3077–3100. (doi:10.1016/j.jmps.2008.05.002)
4. Doyoyo M. 2002 A theory of the densification-induced fragmentation in glasses and ceramics under dynamic compression. *Int. J. Solids Struct.* **39**, 1833–1843. (doi:10.1016/S0020-7683(01)00278-5)
5. Ferri E, Deshpande V, Evans A. 2010 The dynamic strength of a representative double layer prismatic core: a combined experimental, numerical, and analytical assessment. *J. Appl. Mech.* **77**, 061011. (doi:10.1115/1.4000905)
6. Forquin P, Gary G, Gatuingt F. 2008 A testing technique for concrete under confinement at high rates of strain. *Int. J. Impact Eng.* **35**, 425–446. (doi:10.1016/j.ijimpeng.2007.04.007)
7. Adley MD, Frank AO, Danielson KT. 2012 The high-rate brittle microplane concrete model. I. Bounding curves and quasi-static fit to material property data. *Comput. Concrete* **9**, 293–310. (doi:10.12989/cac.2012.9.4.293)
8. Frank AO, Adley MD, Danielson KT, McDevitt Jr HS. 2012 The high-rate brittle microplane concrete model. II. Application to projectile perforation of concrete slabs. *Comput. Concrete* **9**, 311–325. (doi:10.12989/cac.2012.9.4.311)
9. Gailly BA, Espinosa HD. 2002 Modelling of failure mode transition in ballistic penetration with a continuum model describing microcracking and flow of pulverized media. *Int. J. Numer. Methods Eng.* **54**, 365–398. (doi:10.1002/nme.427)
10. Gatuingt F, Pijaudier-Cabot G. 2002 Coupled damage and plasticity modelling in transient dynamic analysis of concrete. *Int. J. Numer. Anal. Methods Geomech.* **26**, 1–24. (doi:10.1002/nag.188)
11. Grady D. 1982 Local inertial effects in dynamic fragmentation. *J. Appl. Phys.* **53**, 322–325. (doi:10.1063/1.329934)
12. Grady D. 1998 Shock-wave compression of brittle solids. *Mech. Mater.* **29**, 181–203. (doi:10.1016/S0167-6636(98)00015-5)
13. Grady D, Kipp M. 1979 The micromechanics of impact fracture of rock. *Int. J. Rock Mech. Mining Sci. Geomech. Abs.* **16**, 293–302. (doi:10.1016/0148-9062(79)90240-7).
14. Grady D, Kipp M. 1995 Experimental measurement of dynamic failure and fragmentation properties of metals. *Int. J. Solids Struct.* **32**, 2779–2791. (doi:10.1016/0020-7683(94)00297-A)
15. Grady DE. 1990 Particle size statistics in dynamic fragmentation. *J. Appl. Phys.* **68**, 6099–6105. (doi:10.1063/1.347188)
16. Kožar I, Ožbolt J. 2010 Some aspects of load-rate sensitivity in visco-elastic microplane model. *Comps. Conc.* **7**, 317–329. (doi:10.12989/cac.2010.7.4.317)
17. Mescall J, Weiss V. 1984 Materials behavior under high stress and ultrahigh loading rates. II. In *Proc. 29th Sagamore Army Conference*. Watertown, MA: Army Materials and Mechanics Center.
18. Mott N. 1947 Fragmentation of shell cases. *Proc. R. Soc. Lond. A* **189**, 300–308. (doi:10.1098/rspa.1947.0042)
19. Ožbolt J, Sharma A, Reinhardt H-W. 2011 Dynamic fracture of concrete – compact tension specimen. *Int. J. Solids Struct.* **48**, 1534–1543. (doi:10.1016/j.ijsolstr.2011.01.033)
20. Shih C, Nesterenko V, Meyers M. 1998 High-strain-rate deformation and comminution of silicon carbide. *J. Appl. Phys.* **83**, 4660–4671. (doi:10.1063/1.367252)
21. Wei Z, Evans A, Deshpande V. 2009 The influence of material properties and confinement on the dynamic penetration of alumina by hard spheres. *J. Appl. Mech.* **76**, 051305. (doi:10.1115/1.3129765)
22. Freund LB. 1990 *Dynamic fracture mechanics*. Cambridge, UK: Cambridge University Press.
23. Shockey DA, Curran DR, Seaman L, Rosenberg JT, Petersen CF. 1974 Fragmentation of rock under dynamic loads. *Int. J. Rock Mech. Sci. Geomech. Abstr.* **11**, 303–317. (doi:10.1016/0148-9062(74)91760-4)
24. Hemmert DJ, Smirnov VI, Awal R, Lati S, Shetty A. 2010 Pulsed power generated shockwaves in liquids from exploding wires and foils for industrial applications. In *Proc. of the 16th Int. Symp. on High Current Electronics, Tomsk, Russia*, pp. 537–540.
25. Maurel O, Reess T, Matallah M, DeFerron A, Chen W, La Borderie C, Pijaudier-Cabot G, Jacques A, Rey-Bethbeder F. 2010 Electrohydraulic shock wave generation as a means to

increase intrinsic permeability of mortar. *Cement Concrete Res.* **40**, 1631–1638. (doi:10.1016/j.cemconres.2010.07.005)
26. Reinhardt HW, Weerheijm J. 1991 Tensile fracture of concrete at high loading rates taking account of inertia and crack velocity effects. *Int. J. Fract.* **51**, 31–42. (doi:10.1007/BF00020851)
27. Bažant ZP, Caner FC. 2014 Impact comminution of solids due to local kinetic energy of high shear strain rate. I. Continuum theory and turbulence analogy. *J. Mech. Phys. Solids* **64**, 223–235. (doi:10.1016/j.jmps.2013.11.008)
28. Caner FC, Bažant ZP. 2014 Impact comminution of solids due to local kinetic energy of high shear strain rate. II. Microplane model and verification. *J. Mech. Phys. Solids* **64**, 236–248. (doi:10.1016/j.jmps.2013.11.009)
29. Bažant ZP, Caner FC. 2013 Comminution of solids caused by kinetic energy of high shear strain rate, with implications for impact, shock, and shale fracturing. *Proc. Natl Acad. Sci. USA* **110**, 19 291–19 294. (doi:10.1073/pnas.1318739110)
30. Su Y, Bažant ZP, Zhao Y, Salviato M, Kirane K. 2015 Viscous energy dissipation of kinetic energy of particles comminuted by high-rate shearing in projectile penetration, with potential ramification to gas shale. *Int. J. Fract.* **193**, 77–85. (doi:10.1007/s10704-015-0019-0)
31. Bažant ZP, Su Y. 2015 Impact comminution of solids due to progressive crack growth driven by kinetic energy of high-rate shear. *ASME J. Appl. Mech.* **82**, 031007. (doi:10.1115/1.4029636)
32. Schuhmann Jr R. 1940 Principles of comminution, I-size distribution and surface calculations. AIME Technical Publication 1189.
33. Caner FC, Bažant ZP. 2012 Microplane model M7 for plain concrete. I. Formulation. *J. Eng. Mech.* **139**, 1714–1723. (doi:10.1061/(ASCE)EM.1943-7889.0000570)
34. Caner FC, Bažant ZP. 2012 Microplane model M7 for plain concrete. II. Calibration and verification. *J. Eng. Mech.* **139**, 1724–1735. (doi:10.1061/(ASCE)EM.1943-7889.0000571)
35. Bažant ZP, Caner FC, Carol I, Adley MD, Akers SA. 2000 Microplane model M4 for concrete. I. Formulation with work-conjugate deviatoric stress. *J. Eng. Mech.* **126**, 944–953. (doi:10.1061/(ASCE)0733-9399(2000)126:9(944))
36. Bažant ZP, Caner FC, Adley MD, Akers SA. 2000 Fracturing rate effect and creep in microplane model for dynamics. *ASCE J. Eng. Mech.* **126**, 962–970. (doi:10.1061/(ASCE)0733-9399(2000)126:9(962))
37. Cargile JD. 1999 *Development of a constitutive model for numerical simulation of projectile penetration into brittle geomaterials*. Report no. SL-99-11. Vicksburg, MS: US Army Engineering Research and Development Center.
38. Bažant ZP, Oh B-H. 1983 Crack band theory for fracture of concrete. *Materials and structures* (*RILEM, Paris*) **16**, 155–177.
39. Červenka J, Bažant ZP, Wierer M. 2005 Equivalent localization element for crack band approach to mesh-sensitivity in microplane model. *Int. J. Numer. Methods Eng.* **62**, 700–726. (doi:10.1002/nme.1216)
40. Bažant ZP, Adley MD, Carol I, Jirasek M, Akers SA, Rohani B, Cargile JD, Caner FC. 2000 Large strain generalization of microplane model for concrete and application. *ASCE J. Eng. Mech.* **126**, 971–980. (doi:10.1061/(ASCE)0733-9399(2000)126:9(971))